

# 3D Hypergraph-Oriented Air Flow Analysis Based On PTV

Denis Klimentjew, Nils Erik Flick, Till Bosselmann, and Jianwei Zhang

*Dept. of Informatics, University of Hamburg, Vogt-Kölln-Straße 30, 22527 Hamburg, Germany*  
{klimentjew, 3flick, 3bosselm, zhang}@informatik.uni-hamburg.de

**Abstract**—The paper introduces a new air flow analysis approach based on Particle Tracking Velocimetry (PTV). One of the special features of the proposed method is that after the tracer particles are detected, matching and tracing are conducted jointly. To this end, we introduce an interpretation module based on a directed hypergraph for 3D curve reconstruction. At first the 2D inter-frame locations are localised and used for the extraction and calculation of 3D keypoints. Through 3D keypoints which are evaluated in several steps by the hypergraph together with the time information, reverse curve matching for path selection can be reconstructed and the resulting trajectories visualized.

In contrast to the preceding work, our approach describes the measuring data by 3D trajectories directly instead of first estimating 2D trajectories and then matching them to 3D trajectories. Even with complicated trajectories, a higher precision can be achieved. A certain independence of the reflections and lighting conditions is reached by interpretation. Moreover, the path of particles can also be reconstructed with the minimum number of 3D keypoints under consideration of path energy minimization.

## I. INTRODUCTION

According to a Dow Jones Newswires prediction, the number of aircraft built by Airbus will double by 2026. The number of passenger aircraft worldwide will approximately be 35,000. Passenger comfort plays an increasingly important role for the marketing of modern aircraft. Therefore, a computer-aided system which evaluates the measurements and visualizes the air-streams inside the cabin would be enormously helpful. The resulting system could assist the developers not only with the prototypes, but also in the assembly of the aircrafts to be modified.

Over the years, several measuring technologies have been discovered. One of the most well-known is based on the use of anemometers which are distributed inside the aircraft [1][2]. For a realistic air-flow model, several anemometers should be placed and calibrated. Moreover, only one dimension of the air-flow is measured and afterwards all data must be merged. As a result, the procedure involves a lot of manpower and time and is cost-intensive.

Furthermore, there are three general categories of methods which measure the velocity of air-flow with the help of tracer particles. Particle Image Velocimetry (PIV) uses a setup consisting of cameras and a laser scanner [3]. As particles pass through the laser illuminated plane, two images are taken within a short period of time. On these images, a cross correlation of image regions is performed in order to obtain the direction and velocity of the flow. This approach is limited by the area which can be illuminated by the laser

as well as the acquisition and transfer rate of the cameras. The main difference between PIV and Hot-wire anemometer respectively Laser Doppler velocimetry techniques is that PIV produces two-dimensional vector fields [4].

The principle idea behind Particle Streak Tracking (PST) is to control the scene illumination through a shutter system [5]. It generates a train of pulses during which the camera is exposed to the reflections of the tracer particles in the scene. For an application of PST for 3D velocity measurement of flows on a single plane see [6]. The PST methods support only a low number of particles. Therefore the resulting information density is rather low. This is a serious handicap for the measurement of turbulent air-flow.

Particle Tracking Velocimetry (PTV) methods identify single particles and track them from frame to frame [7][8]. This makes PTV more suitable for experiments with a low number of particles. The lower number of particles permit depth reconstruction for each particle, provided correspondence can be established. The disadvantages of the methods that deliver a two-dimensional vector field are significant. One of the velocity components (depth direction) is disregarded, some particles and turbulences will not be sufficiently recognised or be totally absent. In other words, the resulting visualization is neither complete nor accurate. Many of the above methods need many hours or even days for the evaluation of measurement data and the visualization of air-flows.

In this paper, we propose a new approach for the evaluation of measurement data and the visualization of air-flows inside the aircraft cabin based on PTV. The setup consists of two synchronised cameras with long exposure time, similar to the setup described in [9] and illustrated in Fig. 1. The helium-filled soap bubbles that are injected through the air-intakes are detected via the stereo camera system. Moreover, the results for the soap bubbles are traced. First, the 2D inter-frame locations of the bubbles are localised and then used for the calculation and extraction of 3D keypoints. The significant difference to the other methods is that the measuring data are described directly by 3D trajectories instead of first estimating the 2D trajectories and then matching them to the 3D trajectories. A higher precision can be achieved even with complicated trajectories. Our method uses reverse curve matching for path selection, so a directed hypergraph is used to evaluate a data-fit term on a curve obtained from a few points resulting from an earlier step.

The hypergraph connects several 3D keypoints through miscellaneous frames and contains time information. In the next step the subpaths are combined. The accruing curves are

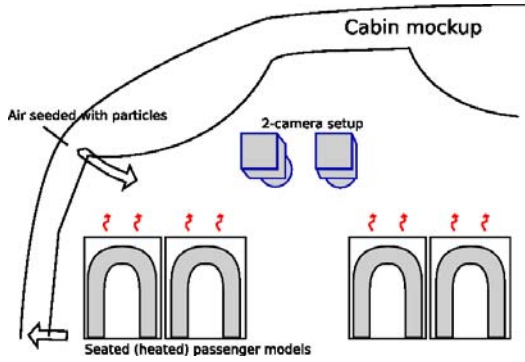


Fig. 1. Cross section of a full-scale aircraft cabin, as used in our experiments.

enhanced with a B-spline under consideration of energy, so-called active contour models. An explanation of the theory can be found in sections III to V.

Independence of the lighting conditions and reflections is reached to a certain degree by interpretation. Moreover, the path of the particles can also be reconstructed with the minimum number of 3D keypoints under consideration of the path energy minimization. Furthermore, the investigated volume is considerably larger than in most other PTV applications.

The rest of this paper is structured as follows. In the next sections we present the theoretical foundations of our method. We describe the applied model, different pre-processing steps, particle segmentation as well as curve fitting and interpretation in sections II to V. Then, in section VI, we describe the experimental setup. The implementation and experimental results are described and discussed in detail. Finally, we present our conclusion in section VII.

## II. PREPROCESSING

The PTV system we developed is based on two synchronised cameras with long exposure time. We used Zhang's calibration method [10] to obtain the camera parameters. As a result of the single camera calibration, we got its intrinsic parameters and the lens distortion. This was done separately for both cameras. After that, we used the semi-automatic calibration method to calibrate the stereo camera system. The transformation matrix between the two cameras' image planes also needs to be determined. There is a wide array of algorithms for this problem. To determine the rectification matrices based on intrinsic and extrinsic camera parameters, we implemented a procedure based on the work of Fusiello et al. [11]. For the background removal an image  $I$  can be seen as the sum of several components:

$$F_{i,f}(\vec{x}) = \alpha \cdot BG_{i,f}(\vec{x}) + N_{i,f}(\vec{x}) + T_{i,f}(\vec{x}) \quad (1)$$

or simplified

$$F_i = T_i + BG_i + N_i \quad (2)$$

where  $F$  denotes the image,  $T_i$  the foreground region containing the traces,  $BG_i$  the background and  $N_i$  the camera noise at frame number  $i$ . In a static scene,  $BG_i$  is affected only by changes in illumination (and reflections). The main

part of  $BG_i$ 's intensity can be removed by calculating a median image over several frames. This template is then subtracted from each input image. If an effort were made to keep illumination constant, the remaining  $BG_i$  intensity would be low enough not to affect further segmentation steps significantly, so that we could assume  $F_i = T_i + N_i$ , which would simplify the following segmentation steps.

## III. PARTICLE SEGMENTATION

Keypoint extraction is too computationally expensive to apply to entire images. In order to obtain regions of interest in which to search for keypoints, region-based segmentation methods are useful.

*Structuring element with hysteresis:* Our first approach was to test for four-connectivity by eroding the binary image with a cross-shaped structuring element. Testing for four-connectivity seemed like a suitable indicator for the presence of traces, as it is unlikely to occur at random ( $\frac{1}{32}$  if  $BG_i$  has been removed and  $N_i$  consists of white noise). The detection rate is strongly dependent on the threshold used to obtain the binary image. The gained regions were then used as starting points to calculate the hysteresis on the original image in order to complete the segmentation result.

*Gradient Magnitude:* Particle traces show a higher gradient magnitude than the surrounding area. For an image  $F(x,y)$ , it is defined as presented below (Eq. 3).

$$|\Delta F(x,y)| = \sqrt{\left(\frac{\delta F(x,y)}{\delta x}\right)^2 + \left(\frac{\delta F(x,y)}{\delta y}\right)^2} \quad (3)$$

This was exploited for segmentation by calculating the gradient magnitude at each pixel and filtering through a threshold  $Tr$ , which was set to a multiple  $n$  of the square root of the variance  $V$ :  $Tr = n * \sqrt{V}$ . We found that changing  $n$  does not change the detection yield significantly. While the algorithm is suitably quick and gradient estimates can be reused for detection, it breaks down on images with low overall variance, leading to too many spurious regions of interest.

*MeanShift:* If  $F$  is viewed as feature space, the MeanShift algorithm can be used for segmentation. It operates by following the density gradient with a kernel in the feature space until a maximum has been reached. Pixels sharing the same gradient maximum are assigned the value of that maximum. All other pixels are assigned the density estimate of the kernel centered at their position. If the kernel is chosen to be suitably large and the noise is uniform and distributed, the method is noise resistant.

Although by no means perfect, the MeanShift based segmentation showed the best performance of all the tested methods due to its suitability for varying classes of input images.

## IV. KEYPOINTS AND CURVE FITTING

First, we will exploit known image structure to obtain a combinatorial representation as a starting point for further analysis. In most points, the projected curve can be approximated as in Eq. 4.

$$\begin{aligned} \Pi(t_a+t) &= h \circ \vec{\zeta}(t_a+t) = \\ &= \Pi'(s) = \vec{\Pi}(t_a) + \frac{\delta \Pi'}{\delta s}(0) \cdot s + \frac{1}{2} \frac{\delta^2 \zeta'}{\delta s^2}(0) \cdot s^2 + O(s^3) \quad (4) \end{aligned}$$

where  $\zeta$  is the space curve,  $h$  the de-homogenization,  $\Pi$  the projected curve and  $\Pi'$  its unit-speed version (parametrized by arc length, since  $t$  is unobservable in practice).

Many methods use templates or intensity maxima for detection and tracking. Going by intensity maxima is not an option for data with long exposure times, because they do not come with a well-defined time stamp; while one could envisage using some formulation of templates (usually contour-based), it seemed more promising in terms of efficiency and also for the sake of parsimony to continue thinking in terms of thickened lines as opposed to regions.

### A. KEYPOINTS

We introduce inter-frame locations of particles as a choice of 2D keypoints, which can be detected on each view individually; the 2D keypoints introduced above are then combined to 3D keypoints, all the while respecting the epipolar constraint. During our initial research, the idea of searching directly for 3D keypoints was rejected because searching, e.g. by masking regions of low contrast and then applying Newton's method to a response function in two dimensions, is less costly in two dimensions than it is in three and, more to the point, there is no essential advantage in doing so (all available *image* information being essentially two-dimensional because it stems from two 2D views, the fundamental ambiguity of epipolar geometry is not resolved by choosing another representation).

Subpixel measurements are introduced naturally in the context of modern image analysis, but we would like to point out that they are not directly responsible for increased precision in our setup; that can be a by-effect, but the main advantage of subpixel-methods is that they allow us to deal more meaningfully with image information. The gain in precision, which is smaller than the apparent radius  $\rho$  of a tracer particle, is in practice smaller than calibration errors which may be of the order of several pixels even in a carefully calibrated setup.

Inter-frame locations are a very good candidate for anchoring further steps because they are well-localized spatially as well as temporally. Furthermore, they are detectable in the image series. At the same time, they can be said to have a standard appearance. The suspicion that inter-frame locations can be detected with high accuracy was confirmed by a test we carried out to investigate whether different *regions* corresponding to background, endings and interiors of thickened lines could be classified with a max-margin linear classifier. As long as there was sufficient contrast, the test turned out successful even within a non-adapted feature space taken from another experiment.

The using of *2D keypoints* as essential significant feature has several advantages:

- They are very robust against the choice of exposure time because the aspect, except for inevitable overlaps, depends only on first order of arclength of the original trajectory, and not on curvature or other aspects of its shape.
- No matter how long the duration of the integration of *intra-frame* information, these keypoints are always equally well localized.

### B. CURVE FITTING

For the software application, the choice fell on Harris' and Stephens' combined edge and corner detector over other possibilities because of excellent localization and high specificity (empirical, synthetic and actual image series), and especially for its avoidance of multiple detections (which would be toxic for the accuracy of measurements). This detector is based on the gradient second-moment tensor, or structure tensor,  $M$ , whose components are image derivatives taken at an inner scale. It is defined as  $hs = \det(M) - k \cdot \text{tr}(M)$  and is a smooth function of location (and scale). When calculated on each (background-subtracted) frame separately, then corroborated between neighbouring frames, it indicates probable intra-frame locations of particles. The fact that it consistently showed better detection rates (lower false-positive, lower false-negative) than an isophote-curvature derived criterion and a detector based on critical points of a certain function calculated on the time-series remains somewhat surprising if one looks at the images.

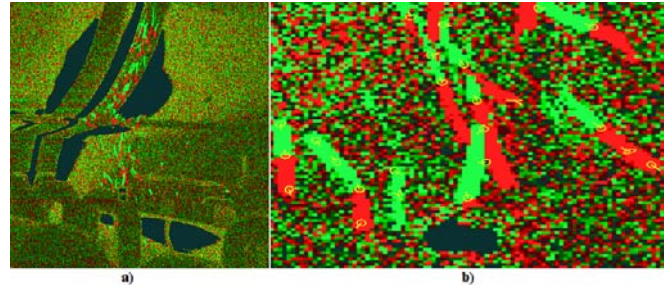


Fig. 2. a) shows the performance of the MeanShift based mask generator with kernel radii of 8. b) is an example of correctly detected inter-frame locations, superposed onto a color-coded difference image.

Because it is a gradient-based detector, it is good at capturing properties which do not change much with exposure time – which are also related to first-order properties, i.e. gradients – and we found that the choice of scales does not have appreciable influence on the localization of the inter-frame position, except in crowded areas. This is because any wandering of the spatial maxima is offset by the requirement that the feature be strong on both frames; distribution of the gradient is locally symmetrical at the inter-frame location, as predicted by the model. Fig. 2 shows an example.

## V. INTERPRETATION AND CURVE APPROXIMATION

As mentioned before, the epipolar constraint is a soft constraint in the analysis of actual stereo image data, in the

sense that some tolerance must be allowed for. This circumstance can even be leveraged to compensate imperfections in calibration; indeed, for every matching which is made between 2D keypoints, the image is subsequently locally subjected to an affine warping, according to the average offset normal to the epipolar lines, which approximates the local effects of a re-calibration “as if the matchings were confirmed”. In this way, intra-frame observations are not lost even if calibration is less than perfect, and moderate calibration errors do not result in non-detection, only in a predictable error in the estimation of velocities.

Keypoints appearing on consecutive frames might belong to the same particle. However, which 3D keypoints actually correspond to particle locations is not known beforehand because of the epipolar matching ambiguity, and which continuations correspond to particle trajectories is not known either. For that reason, an immediate interpretation is not possible; it is necessary to take intra-frame observations into account at this point. These are not timestamped and we know only that they were accumulated between the instants  $T \cdot i$  and  $T \cdot (i + 1)$ , and furthermore we know the temporal ordering because we regard a particle trace as a blurred line.

#### A. INDIRECT ANALYSIS

It is true that the 3D keypoints are already furnished with a tangent direction for each view except when the motion is exactly along an optical ray, which occurs almost never, and which determines the direction in 3D except for a motion inside an epipolar plane (i.e., each keypoint is a point in  $\mathbb{R}^4 \times \mathbb{RP}^1 \times \mathbb{RP}^1$ ), which makes a preferred search direction plausible. However, extrapolation, with moderate exposure times, is not possible especially in the case where turbulent motion is resolved and even so, it can only serve to reduce the number of possible candidates.

In the following, we always assume that all interframe locations which are detectable with sufficient confidence have been detected. While it might be possible to achieve good results by suitably tracing out the trajectories from image information, we think it preferable not to proceed in this direct way but instead to generate hypotheses and filter them according to how well they explain the frame content. This circumvents most problems local path-following methods have with ambiguous situations, especially in the presence of occlusion.

The advantages over indirect analysis via hypotheses are manifest:

- Thanks to a global, top-down view, results are much less likely to be influenced by local fluctuations, noise and difficult situations (i.e. crossings of traces) than local approaches.
- There are enhanced opportunities for a true probabilistic interpretation of the image series, as explained below.
- One can unambiguously fit simple curves to just a few keypoints, which nevertheless remain accurate to a high order if desired (B-splines lend themselves to it).

The third point above can be understood as an instance of Occam’s Razor; moreover, it renders optimization over curve

spaces completely unnecessary.

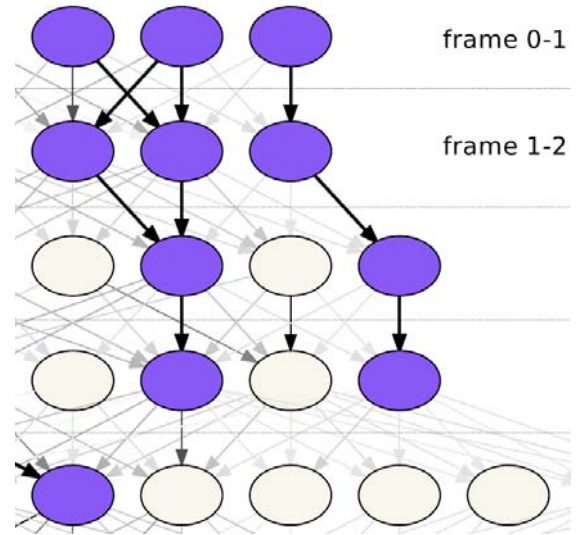


Fig. 3. Directed graph of continuations.

All possible immediate continuations form an acyclic, directed graph (Fig. 3). We extend it to a directed hypergraph by considering all paths up to an arbitrary number of frames  $f$ .  $f$  can be small, of the order of about 5 frames, and longer range dependencies are disregarded, because the particle motion can be described locally. By cutting hyperedges (e.g. bottom-up, by removing edges first and enforcing transitivity under these constraints), one can partition the hypergraph of continuations into non-branching segments. These partitions are possible *explanations*, or *interpretations*, of the image evidence  $g$  and should be assigned a probability.

$$p(\beta|g) = \frac{p(g|\beta)p(\beta)}{p(g)} \quad (5)$$

An application of the Bayes theorem: in Eq. 5,  $\beta$  represents the curve parameters and  $g$  the image evidence. The prior distribution  $p(\beta)$  can be chosen on physical grounds; for example, one should favor interpretations which do not require excessive kinetic energy to realize.  $p(\beta|g)$  would be read as the probability of a single trajectory being supported by the image evidence; the probability of the whole hypergraph partitioning depends on the individual trajectories’ probabilities, which are independent except for the interdiction of crossings and for the handling of subchains.

In our implementation of the framework,  $p(g|\beta)$  is replaced by any of a set of criteria for good fit, ideally a monotonically increasing function of the actual probability, while the hypergraph partitioning itself is carried out by a greedy algorithm, which orders the possible trajectories by their score and discards all but the best one in ambiguous situations (proceeding recursively from longer chains to subchains).  $p(g)$  is irrelevant, because we are mostly interested in relative probabilities; A unified way of determining a threshold for any of the scores so as to reject bad explanations (in case no path is viable) would be a topic for further research.

## B. CURVE APPROXIMATION

The problem of interpreting the images is thus reduced from a problem properly involving an integration over continuous probability distributions to the purely combinatorial question of finding the chains of keypoints which correspond to actual particle traces, reducing the search space to a realistic size by arguing that all sensible curves which contribute most to the probability of a path look about the same and can be reduced to a point estimate.

Each path candidate (chain) from the hypergraph is converted to a smooth trajectory candidate by means of B-splines. As alluded to above, B-splines play a simplification role. On the one hand, a detail which cannot be resolved when measuring is not spuriously resolved in the description (since B-spline spaces with few knots do not allow for it), and overfitting does not occur; on the other hand, they approximate data well (the approximation of a smooth function is accurate to a high order). Note that B-splines are not suited for extrapolation. This is not a disadvantage in our application.

## VI. APPLICATION DEVELOPMENT AND EVALUATION

### A. REAL EXPERIMENTAL SETUP

Frames  $\{F_{i,f}\}$  captured by camera number  $i$  at frame number  $f \in \{0, \dots, f_{max}\}$  are images obtained by the cameras sensors integrating from  $\frac{f}{frame\ rate}[s]$  to  $\frac{f}{frame\ rate} - gap[s]$  along the time axis. The gap during which the sensor is not exposed should be as short as possible; it is always disregarded in the remainder of the text. In our setup, the camera positions are fixed with respect to an immobile scene. The backgrounds overall brightness may vary because of oscillations in lighting intensity (indeed, fluorescent lamps might serve as light sources) which flicker at a frequency usually out of tune with the imaging system. This should not throw off our system, and indeed in the experiments it did not, even without more sophisticated background subtraction.

### B. IMPLEMENTATION

In order to evaluate the system, an application was programmed in C++, using data structures and algorithms from the VIGRA library for image processing. Aside from an implementation of the detection and tracking algorithm, a GUI was built using the QT library which contains a visualization widget based on the VTK library. The application can visualize detected particle trajectories and a model of the experimental environment in 3D. The overall structure of the application can be seen in Fig. 4. Each feature is implemented as a separate widget. The detection and rectification steps are assigned their own threads, in order to keep the GUI operational while they are processing images. While the system can work on wholly rectified images, as indicated in Fig. 4, it is also able to rectify (and free from distortion) single points. Considering that neither rectification nor freedom from distortion are necessary for the particle segmentation and keypoint extraction, this yields a considerable performance gain. Rectification is, however,

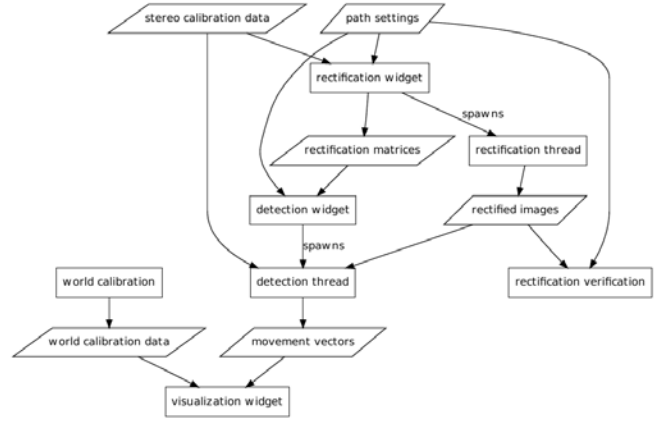


Fig. 4. Illustration of the implementation of the system. Data is denoted by parallelograms, and processing components by rectangles.

crucial for an efficient correspondence search as it facilitates the search for correspondences on the scanlines of image pairs. The application is equipped with a widget to allow the user to visually evaluate the quality of the rectification (and in extension of the stereo calibration).

Our PTV system calculates the positions of the particle trajectories relative to one of the cameras, and not in the world coordinate system. As knowledge of the latter position is required for a meaningful interpretation of the measurements, a widget is provided to assist the user in obtaining the necessary transformation between the two. This is done by calculating the absolute orientation between two sets of points from either system. The user is required to manually establish the correspondences.

### C. EXPERIMENTAL RESULTS

The implemented application comprises temporal information and the reconstructed 3D particle trajectories. In spite of the foundations described in V the temporal information can be determined through the synchronized cameras and particle traces (blurred lines).

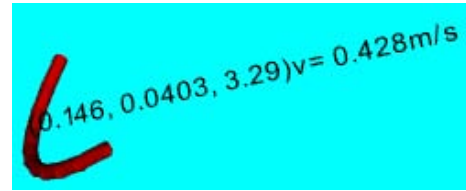


Fig. 5. Visualization of air-flow velocity with numerical indicators placed directly on the reconstructed 3D trajectories.

To compute the velocity of single particles we use two different algorithms, the above-mentioned physical properties or the first derivative of the resulting curvature. To assist the developers of air conditioning systems, we use different means for the visualization of the velocity of the particles. For the visualization of single particles the direct numerical indicator (shown in Fig. 5) can be used. For a large number of particles, the color-coded visualization of the velocities is advantageous. Fig. 6 shows the color and hue coded

trajectories of the particles; the slowest particles are green, the fastest are red (color and hue coded).

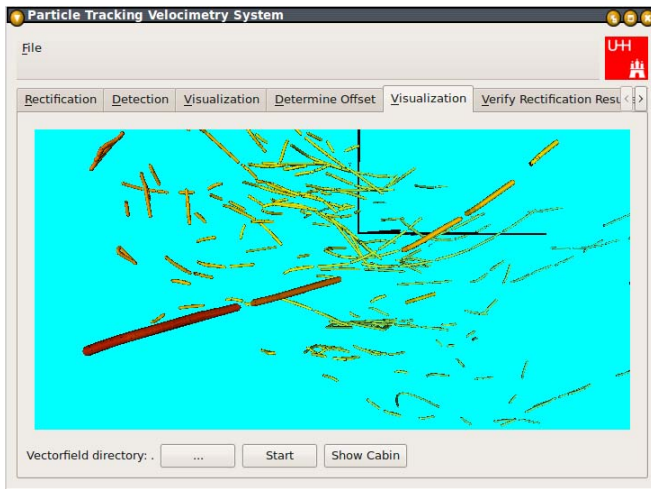


Fig. 6. Color and hue coded velocities of reconstructed 3D trajectories. The slowest particles are green, the fastest are red.

Exact evaluation of fluid experiments needs ground truth, which is not always easily obtainable: however, for validation, one can resort to synthetic images, employing ray tracing in order to use the observational model as a generative model. Experimental results are encouraging: the detection



Fig. 7. Trajectory accurately reconstructed from synthetic image series.

process, when run on a synthetic image series showing a portion of a circular motion, reports only two candidates for motion after hyperedge selection, one corresponding closely to the true motion (with very low average deviation of ca. 1%), see Fig. 7. The system was also subjected to a

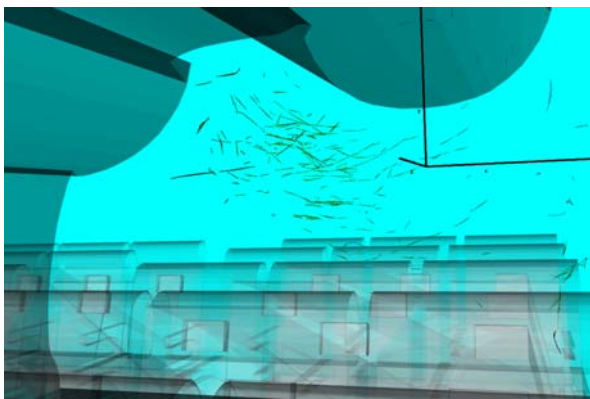


Fig. 8. Detected particle trajectories shown in a model of the environment. series of tests in an industrial environment for which prior measurements with a different system were known. As it was not feasible to obtain the ground truth, it is impossible

to calculate an error. However, the velocity distribution and overall flow orientation matched expectations. The measurement result of one of the test series is shown in Fig. 8. An image series of 1000 frames from each camera takes ca. 1500s on a 1.6GHz computer. The system scales linearly with the number of frames.

## VII. CONCLUSION

This work demonstrated that depth reconstruction of sparse flow information is practical using a stereo camera setup. Furthermore, tracking of individual particles can be done by generating a graph of possible paths and matching generated curves.

To sum up, the direct description of the measuring data by 3D trajectories instead of first estimating the 2D trajectories and matching them to 3D trajectories is revealed as advantageous. To the best of our knowledge this is the first approach to develop a depth recovering particle velocimetry system, which can operate under fairly broad conditions, such as requiring only the use of a stereo camera setup and a low sampling frequency. A higher precision can also be achieved with complicated trajectories. The presented system is capable of making essentially one-dimensional measurements of a fully 3 + 1 - dimensional spatio-temporal phenomenon. The fact that these measurements are subject to a number of uncertain factors is known and noted; the uncertainty, as presented in the main text, can be estimated to a certain extent and that information is available for every individual measurement.

## REFERENCES

- [1] P. C. Stainback, K. A. Nagabushana, Review of Hot-Wire Anemometry Techniques and the Range of their Applicability for Various Flows, *Electronic Journal of Fluids Engineering* 119, 1997
- [2] F. K. Owen, A. K. Owen, Measurement and assessment of wind tunnel flow quality, *Progress in Aerospace Sciences* 44, Elsevier Ltd., 2008
- [3] G. Guenther, J. Bosbach, J. Pennecot, C. Wagner, T. Lerche, and I. Gores, Experimental and numerical simulations of idealized aircraft cabin flows, *Aerosp Sci Technol* 10, pp 563-573, 2006
- [4] J. Bosbach, M. Kuehn, and C. Wagner, Large scale particle image velocimetry with helium filled soap bubbles, *Experiments in Fluids* 46, no. 3, pp 539-547, 2009
- [5] Y. Zhang, Y. Sun, A. Wang, JL Topmiller, JS Bennett, Experimental characterization of airflows in aircraft cabins, Part II: Results and research recommendations, *ASHRAE transactions* 111, pp 53-59, ISSN 0001-2505, 2005
- [6] D. Mueller, B. Mueller, and U. Renz, Three-dimensional particle-streak tracking (PST) velocity measurements of a heat exchanger inlet flow A new method to measure all three air-flow velocity components in a plane is applied to a steady-state three-dimensional flow, *Experiments in Fluids* 30, no. 6, pp 645-656, 2001
- [7] H.-G. Maas, A. Gruen, and D. Papantoniou, Particle tracking velocimetry in three-dimensional flows, Part A, *Exp. Fluids*, 15, 1993
- [8] A. Wang, Y. Zhang, Y. Sun, X. Wang, Experimental study of ventilation effectiveness and air velocity distribution in an aircraft cabin mockup, *Building and Environment*, Vol. 43, Iss. 3, pp 337-343, 2008
- [9] J. Bosbach, M. Kuehn, C. Wagner, M. Raffel, C. Resagk, R. du Puits, and, A. Thess, Large scale particle image velocimetry of natural and mixed convection, 13th Int. Symp. on Applications of Laser Techniques to Fluid Mechanics, Lisbon, Portugal, 2006
- [10] Z. Zhang, A flexible new technique for camera calibration, In: *IEEE Trans. on Pattern Analysis and Machine Intelligence*, 2000
- [11] A. Fusiello, E. Trucco, and A. Verri, A compact algorithm for rectification of stereo pairs, In: *Machine Vision and Applications*, Springer, 2000